

Fluid-Fluid and Fluid-Solid transitions in the Kern-Frenkel model from Barker-Henderson thermodynamic perturbation theory

Christoph Gögelein*

Max-Planck-Institute for Dynamics and Self-Organization (MPIDS), 37077 Göttingen, Germany

Flavio Romano†

Physical and Theoretical Chemistry Laboratory, Department of Chemistry,

University of Oxford, Oxford OX1 3QZ, United Kingdom

Francesco Sciortino‡

Dipartimento di Fisica and CNR-ISC, Sapienza Università di Roma,

Piazzale A. Moro 5, 00185 Roma, Italy

Achille Giacometti§

Dipartimento di Scienze dei Materiali e Nanosistemi, Università Ca' Foscari Venezia,

Calle Larga S. Marta DD2137, I-30123 Venezia, Italy

(Dated: August 8, 2018)

Abstract

We study the Kern-Frenkel model for patchy colloids using Barker-Henderson second-order thermodynamic perturbation theory. The model describes a fluid where hard sphere particles are decorated with one patch, so that they interact via a square-well (SW) potential if they are sufficiently close one another, and if patches on each particle are properly aligned. Both the gas-liquid and fluid-solid phase coexistences are computed and contrasted against corresponding Monte-Carlo simulations results. We find that the perturbation theory describes rather accurately numerical simulations all the way from a fully covered square-well potential down to the Janus limit (half coverage). In the region where numerical data are not available (from Janus to hard-spheres), the method provides estimates of the location of the critical lines that could serve as a guideline for further efficient numerical work at these low coverages. A comparison with other techniques, such as integral equation theory, highlights the important aspect of this methodology in the present context.

PACS numbers: 64.75.Gh,82.60.Lf,82.70.Dd

Keywords: Phase separation, Thermodynamics of solutions, Colloids

*Electronic address: christoph.goegelein@ds.mpg.de

†Electronic address: flavio.romano@gmail.com

[‡]Electronic address: francesco.sciortino@uniroma1.it

[§]Electronic address: achille@unive.it

I. INTRODUCTION

Perturbation theory has a long and venerable history in the context of fluids and a detailed description of several different techniques is presented in classic textbooks [1, 2], and in excellent dedicated reviews [3, 4].

Although the general idea dates back to a much earlier time, the first well established paradigm of first- and second-order perturbation theory was devised by Zwanzig [5] for simple fluids, later extended to polar fluids [6]. A similar analysis was carried out by Buff and Schindler in the context of solution theory [7].

In addition to these theories that assume the hard-spheres model as unperturbed system, other theories exist that rely on the van der Waals picture as a starting point, the best known of these being the Weeks-Chandler-Anderson (WCA) theory [8–11].

While the WCA theory has proven extremely powerful in many applications, for potential with hard-cores the original Zwanzig theory offers a natural scheme, hinging on an unambiguous potential separation. This was eventually put on firm ground by Barker and Henderson (BH) [3, 4, 12] who provided reliable estimates for square-well fluids [13], a rather unrealistic potential in the framework of simple liquids, but much more physically sound when applied to the colloid domain.

In the present paper, we will apply the BH thermodynamic perturbation theory to the Kern-Frenkel (KF) model for patchy colloids [14, 15]. In this model [14], attractive circular patches are distributed on the surface of hard-spheres, and different spheres attract each other provided that any two patches on distinct spheres are suitably aligned, and the relative radial distance between the centers of the spheres is within the range of the attractive tail.

While not new [16], these systems have witnessed an impressive resurgence of interest in the last few years for a number of reasons. The first reason is due to the remarkable improvements in the chemical synthesis techniques that allows to decorate the surface of a colloid with great precision and reliability, a feature that was not possible until few years ago. When combined with the additional advantage, as compared with their atomic counterpart, of an almost arbitrarily control of their size and interaction range, this makes patchy colloids very attractive for technological applications, as elementary building blocks for self-assembly materials of the new generation [17, 18]. An additional important reason hinges on the fact that patchy colloids may serve as a paradigm for systems with low valence, strong anisotropy, and highly directional interactions between particles, a feature that is common to many different systems, globular proteins being a notable example,

where the heterogeneity of the surface groups cannot be neglected even at the minimal level.

Several examples of applications and improvements of the original BH scheme have been offered over the years. Verlet and Weiss discussed a comparison with numerical simulations and experimental results both for simple [19] and polar [20] fluids; Gubbins and Gray [21] proposed a perturbation scheme for molecular fluids; Chang and Sandler [22] exploited it to develop an analytical approximation for the square-well fluid valid within a particular interval of well amplitude; Zhang et al, [23] applied it to a square-well chain fluid, whereas Rotemberg *et al.* [24] used it to study the phase behavior of mixtures of colloidal particles and interacting polymers. More recently, Zhou [25] derived a simple procedure hinging on the BH scheme to locate the fluid-solid coexistence phase for a hard-core attractive Yukawa fluid, and Kalyuzhnyi *et al.* [26, 27] tackled the single and multiple patchy colloids, similar to those treated in the present work, using a generalization of Wertheim's thermodynamic perturbation theory [28–31].

The present work builds upon the methodology outlined in Ref. [32] to show that BH second-order perturbation theory can be successfully applied to patchy colloids, as represented by the Kern-Frenkel model [14]. Besides thermodynamic quantities, such as virial equation of state and chemical potentials, the method allows a rather precise location of the fluid-fluid and the fluid-solid coexistence lines, in principle for arbitrary number and size of the patches. In this respect, the method competes in accuracy with integral equation theory on the same system [33, 34], without suffering from the unavoidable instabilities present in that case for low surface coverages and temperatures. This will be demonstrated by an explicit comparison with numerical simulations carried out [33–36] on the same system.

The outline of the paper is as follows. In Section II the model is defined and in Section III the used perturbation technique is described. Some technical details of the calculations are included in Appendices A and B. Section IV includes the method to compute the coexistence curves from the analytical results, with details of the numerical procedure included in Appendix C. Section V briefly summarize some details of the Monte Carlo calculations, and Section VI includes descriptions of all results. Finally, Section VII summarizes the paper and provides some future perspectives.

II. THE KERN-FRENKEL MODEL

Consider a fluid formed by N particles in a volume V at temperature T , and assume that they can be described by the Kern-Frenkel model [14] in its one-patch version (see Fig. 1), where the orientation of the patch on each surface sphere 1 and 2 is identified by unit vectors $\hat{\mathbf{n}}_1$ and $\hat{\mathbf{n}}_2$,

whereas the direction connecting centers of spheres 1 and 2 are identified by unit vector $\hat{\mathbf{r}}_{12}$.

Two spheres of diameter σ attract via a square-well potential of width $(\lambda - 1)\sigma$ and depth ϵ if the directions of the patches on each sphere are within a solid angle defined by θ_0 , and repel each other as hard spheres otherwise. The pair potential has the form

$$\Phi(12) = \phi_0(r_{12}) + \Phi_I(12), \quad (2.1)$$

where the first term is the hard-sphere contribution

$$\phi_0(r) = \begin{cases} \infty, & 0 < r < \sigma \\ 0, & \sigma < r \end{cases}, \quad (2.2)$$

and the second term

$$\Phi_I(12) = \phi_{\text{SW}}(r_{12}) \Psi(\hat{\mathbf{n}}_1, \hat{\mathbf{n}}_2, \hat{\mathbf{r}}_{12}) \quad (2.3)$$

is the orientation-dependent attractive part which can be factorized into an isotropic square-well tail

$$\phi_{\text{SW}}(r) = \begin{cases} -\epsilon, & \sigma < r < \lambda\sigma \\ 0, & \lambda\sigma < r \end{cases}, \quad (2.4)$$

multiplied by an angular dependent factor

$$\Psi(\hat{\mathbf{n}}_1, \hat{\mathbf{n}}_2, \hat{\mathbf{r}}_{12}) = \begin{cases} 1, & \text{if } \hat{\mathbf{n}}_1 \cdot \hat{\mathbf{r}}_{12} \geq \cos \theta_0 \quad \text{and} \quad -\hat{\mathbf{n}}_2 \cdot \hat{\mathbf{r}}_{12} \geq \cos \theta_0 \\ 0, & \text{otherwise} \end{cases}. \quad (2.5)$$

The unit vectors $\hat{\mathbf{n}}_i(\omega_i)$, ($i = 1, 2$), are defined by the spherical angles $\omega_i = (\theta_i, \varphi_i)$ in an arbitrarily oriented coordinate frame and $\hat{\mathbf{r}}_{12}(\Omega)$ is identified by the spherical angle Ω in the same frame. Reduced units, for temperature $T^* = k_B T / \epsilon$, pressure $P^* = \beta P / \rho$ and density $\rho^* = \rho \sigma^3$, will be used throughout, with k_B being the Boltzmann constant. For future reference, we also introduce the packing fraction $\eta = \pi \rho^* / 6$. Two particles then attract if they are within the range of the square-well potential and if their attractive surfaces are properly aligned with each other, and repel as hard spheres otherwise.

The relative ratio between attractive and total surfaces is the coverage χ that is related to the semi-angular width θ_0 of the patch. This can be obtained as

$$\chi^2 = \langle \Psi(\hat{\mathbf{n}}_1, \hat{\mathbf{n}}_2, \hat{\mathbf{r}}_{12}) \rangle_{\omega_1 \omega_2} = \langle \Psi^2(\hat{\mathbf{n}}_1, \hat{\mathbf{n}}_2, \hat{\mathbf{r}}_{12}) \rangle_{\omega_1 \omega_2} = \sin^4 \left(\frac{\theta_0}{2} \right), \quad (2.6)$$

where we have introduced the angular average

$$\langle \dots \rangle_{\omega} = \frac{1}{4\pi} \int d\omega \dots \quad (2.7)$$

III. BERKER-HENDERSON PERTURBATION THEORY

The Kern-Frenkel potential defined in Eqs. (2.1), (2.2), (2.3), (2.4), and (2.5), leads to the natural separation into a reference one (the hard-sphere contribution) and an interaction term (the remaining, angular dependent, part) that is usually requested by the standard perturbation theory prescription [1, 2].

The presence of the hard-sphere potential for the reference part further suggests the Barker-Henderson (BH) scheme [12] as the most suitable one for the present model. This has also the additional advantage that the free energy F_0 for the reference system can then be computed in several ways, as further discussed below.

The original scheme, due to Zwanzig [5], provided the first and second-order terms within the canonical ensemble, in the form of a high temperature expansion

$$\frac{\beta(F - F_0)}{N} = \frac{\beta F_1}{N} + \frac{\beta F_2}{N} + \dots, \quad (3.1)$$

where the first term is proportional to $1/T^*$, the second to $(1/T^*)^2$.

Although formally correct, it was noticed by Barker and Henderson [3, 4, 12] that the corresponding expressions were not useful for finite systems and a grand canonical ensemble derivation provided a much more convenient framework, where the results for the canonical ensemble could be eventually obtained by a Legendre transformation.

To the best of our knowledge, the details of the computation for the second-order term were presented in Ref. 3 only for isotropic potentials. As its generalization to angular dependent potentials proves to be instructive, we have outlined in Appendix A.

The first term poses no problem and is computed in Eq.(A18). When the perturbation parameter $\gamma = 1$ and particularized to the Kern-Frenkel potential given in Eqs. (2.1), (2.2), (2.3), (2.4), and (2.5) it becomes

$$\frac{\beta F_1}{N} = \frac{12\eta}{\sigma^3} \int_{\sigma}^{\lambda\sigma} dr r^2 g_0(r) \phi_{\text{SW}}(r) \langle \beta \Psi(12) \rangle_{\omega_1, \omega_2}. \quad (3.2)$$

Note that this term is negative because so is $\phi_{\text{SW}}(r)$.

The second term is much more involved, but one can apply the same procedure as the isotropic case [32], as detailed in Appendix A. The result for the second term is reported in Eq.(A19). As in the isotropic case, however, this derivation is of little practical use in view of the presence of the three and four point distribution functions [3]. Barker and Handerson [12], devised then a simpler procedure to compute this term, based on a discrete representation of the radial axis distributions.

Again, the original procedure for spherically symmetric potentials is extended to angular dependent potentials in Appendix B.

The result for the second-order term is reported in Eq.(B14). In case of the Kern-Frenkel potential, it yields

$$\frac{\beta F_2}{N} = -\frac{6\eta}{\sigma^3} \left(\frac{\partial \eta}{\partial P_0^*} \right)_T \int_{\sigma}^{\lambda\sigma} dr r^2 g_0(r) \phi_{\text{SW}}^2(r) \left\langle [\beta \Psi(12)]^2 \right\rangle_{\omega_1, \omega_2}, \quad (3.3)$$

where $P_0^* = \beta P_0 / \rho$ is the reduced pressure of the HS reference system in the Carnahan-Starling approximation [37].

This result is identical to that reported in Ref. [32] for a different radial part and it is known as *macroscopic compressibility approximation* [12]. Although the results given in Eqs.(3.2) (first order) and (3.3) (second order) are somewhat intuitive, being the natural extensions of the isotropic counterpart, a detail analysis of their derivations is important as it might help to improve a drawback of the method that will be discussed at the end of Section IV.

IV. FLUID-FLUID AND FLUID-SOLID COEXISTENCE CURVES

Once the reduced free energy per particle $\beta F/N$ is known, all thermodynamic properties can be derived. In particular, the pressures and the chemical potentials can be derived from the standard thermodynamic identities [1]

$$\frac{\beta P}{\rho} = \eta \frac{\partial}{\partial \eta} \left(\frac{\beta F}{N} \right) \quad (4.1)$$

$$\beta \mu = \frac{\partial}{\partial \eta} \left(\eta \frac{\beta F}{N} \right). \quad (4.2)$$

The gas-liquid (fluid-fluid) and fluid-solid coexistence curves are determined by the equality of the temperature, pressure and chemical potential in the two coexisting phases. Since the two phases are in contact, the condition on the equality of the temperature is always fulfilled. Thus, at fixed temperature T^* , we are left with the two conditions on the pressure and chemical potential.

For the gas-liquid coexistence, the conditions are

$$P_g^*(T^*, \rho_g^*) = P_l^*(T^*, \rho_l^*) \quad (4.3)$$

$$\mu_g^*(T^*, \rho_g^*) = \mu_l^*(T^*, \rho_l^*), \quad (4.4)$$

where subscripts g, l indicate that the quantity is computed in the gas and liquid phase respectively. The solution of this system of non-linear equation gives $\rho_g^* = \rho_g^*(T^*)$ for the gas coexistence branch, and $\rho_l^* = \rho_l^*(T^*)$ for the liquid coexistence branch. The hard-sphere reference part of the free energy

(in excess with respect to the ideal gas) is assumed to be described by the Carnahan-Starling relation [37]

$$\left[\frac{\beta F_0}{N} \right]_{\text{liquid}} = \frac{4\eta^2 - 3\eta^3}{\eta(1-\eta)^2}. \quad (4.5)$$

For the hard-sphere radial distribution function $g_0(r)$ part appearing in Eqs. (3.2) and (3.3) the Verlet-Weis [19, 38] corrected Percus-Yevick solution [39, 40] is exploited. The details of the numerical procedure are reported in Appendix C.

A similar method can be applied to the fluid-solid transition, resulting into the conditions

$$P_f^*(T^*, \rho_f^*) = P_s^*(T^*, \rho_s^*) \quad (4.6)$$

$$\mu_f^*(T^*, \rho_f^*) = \mu_s^*(T^*, \rho_s^*). \quad (4.7)$$

All calculations assume that the solid phase retains the crystal structure of the reference system, namely the face-centered cubic (fcc) lattice. It is possible, especially at low T or low χ where anisotropy effects are more relevant, that fcc is not the most stable solid for the model; our coexistence results are still valid, although possibly relating to a metastable solid phase. We used Wood's equation [41]

$$\left[\frac{\beta F_0}{N} \right]_{\text{solid}} = 2.1306 + 3 \ln \left(\frac{\eta}{1 - \eta/\eta_{cp}} \right) + \ln \left(\frac{\rho \Lambda^3}{\eta} \right) \quad (4.8)$$

for the solid free energy of the reference hard-sphere part, where $\eta_{cp} = \pi\sqrt{2}/6$ is the fcc volume fraction for closed packing. For $g_0(r)$ in the solid phase, we use the orientation-averaged pair distribution function of Kincaid and Weis [42].

As a double check of the reliability of the numerical solution of Eqs.(4.6) and (4.7), the critical points were also computed using the alternative, and more direct method, as a maxima of the Helmholtz free energy, that is from the system

$$\frac{\partial^2}{\partial \rho^{*2}} \left(\frac{\beta F}{N} \right) = 0 \quad (4.9)$$

$$\frac{\partial^3}{\partial \rho^{*3}} \left(\frac{\beta F}{N} \right) = 0. \quad (4.10)$$

The solution provides T_c^* and ρ_c^* and are consistent with previous results, as they lay exactly on the top of the coexistence curves.

V. MONTE CARLO SIMULATIONS

Standard Monte Carlo (MC) simulations in the NPT and in the grand-canonical (GC) ensembles have been implemented to evaluate the equation of state and the density dependence of the chemical potential for both the Janus and the SW model. Translational and rotational moves consist of random translation of $\pm 0.1\sigma$ and random rotation of ± 0.1 rad of a randomly selected particle. In the GC study, insertion and deletion moves have been attempted, in average, every 500 displacement moves. In NPT simulations, $N = 500$ particles were investigated. In GC simulations box sizes were selected in such a way that the number of particles in the simulation box would always be larger than 500. Fluid-fcc coexistence lines were calculated via Gibbs-Duhem integration [43], starting from initial coexistence values at $T^* = 2$ established via direct coexistence methods [44]. Since at infinite temperature the KF model reduces to the hard sphere model, coexistence pressures at $T^* = 2$, a very high value for the KF model, were searched for in the vicinity of the known HS values. We refer the reader to Refs. [44, 45] for the details of the procedures. We point out that all *NPT* simulations of the fcc solid were carried out in a cubic box to constrain the system to retain the fcc arrangement also in cases where the preferred structure would be a different one, possibly other lattices or a distorted fcc. This choice was made to properly compare simulation results with the perturbation theory that assumes the cubic fcc arrangement of the reference SW system.

VI. RESULTS

A. Equation of state and chemical potential

In order to assess the performance of perturbation theory, we first compare results for pressure and chemical potential as derived from the BH scheme outlined in Sect.III, with numerical simulations [33–36]. These values were further compared with those derived in Ref. [33, 34] from integral equation (IE) theory within the reference hypernetted chain (RHNC), following the method devised by Lado [46–48]. In the square-well case, integral equation values were taken from Ref.[49].

The results are shown in Figures 2 (pressure) and 3 (chemical potential), for two representative values of the coverages, namely the square-well ($\chi = 1$) (top panels) and the Janus ($\chi = 0.5$) (bottom panels). In all cases, a value of $\lambda = 1.5$ for the total extension of the well (in units of the hard-spheres diameter), was selected in order to compare with previous results.

In the square-well case (top panels), the first selected temperature $k_B T/\epsilon = 1.4$ corresponds

to a temperature above the critical temperature, while the last one $k_B T/\epsilon = 1.0$ is well below (see Ref.[49] and references therein). In both cases, the performance of the BH thermodynamic perturbation theory is remarkably good, in agreement with previous findings on the square-well potential [13]. The dip in the curve for $k_B T/\epsilon = 1.0$ indeed corresponds to the van der Waals loop typical of the coexistence region. In the case of chemical potential (Fig.3), the ideal gas low density solution $\beta\mu = \ln(\rho\sigma^3)$ is also reported for comparison. Interestingly, while both Monte Carlo (MC) simulations and RHNC integral equation theory (IE) converge to the correct limit, the BH perturbation theory appears to underestimate the chemical potential in the whole range of densities. On the other hand, it provides the same quality results for all temperatures, even in those regions where integral equation theory are known to experience difficulties.

Slightly less satisfactory results are obtained in the case of a Janus fluid, as shown in the bottom panels of both Figs. 2 and 3. Here the two limiting temperatures $k_B T/\epsilon = 0.9$ and $k_B T/\epsilon = 0.55$ are both above the critical temperature [36], as apparent from the absence of any loop in both the pressure and the chemical potential. The Janus phase diagram, however, is known to be anomalous [35], as a result of a competition with a micelle formation process that destabilizes the condensation one [36]. In this case the BH thermodynamic perturbation theory (BH) does not show a well defined pattern as it overestimates the pressure for both temperatures (Fig.2 bottom panel), as well as the chemical potential for $k_B T/\epsilon = 0.55$, but underestimates it for the higher temperature $k_B T/\epsilon = 0.9$ (Fig. 3 bottom panel). While it is known that the BH compressibility approximation can be expected to display different performance at different densities due the presence of higher-order terms [12], the above behavior is more likely to be attributed to the anomalous behavior of the Janus phase diagram that perturbation theory cannot capture at the present stage. In spite of this, the performance of BH thermodynamic perturbation theory remains remarkable, especially in view of the difficulties experienced by integral equation theories at such low temperatures associated with low surface coverages.

B. The fluid-fluid coexistence

A very stringent test on the reliability of BH thermodynamic perturbation theory stems from the calculation of the fluid-fluid (gas-liquid) coexistence curves. This is depicted in Figure 4 where the coexistence curves are computed by BH thermodynamic perturbation theory (solid lines), and contrasted with results from Monte Carlo numerical simulations (points), from Ref. [36]. The considered coverages range from $\chi = 1.0$, corresponding to the SW fluid, to $\chi = 0.5$, corresponding

to the Janus limit, and are identical to those considered in Ref.[36]. As before, $\lambda = 1.5$ was assumed in all calculations. In the BH thermodynamic perturbation theory, further coverages down to the hard-sphere limit were also computed. In all cases, the critical points stemming from the BH calculations are also displayed as solid circles on the binodals.

The performance of the BH method appears to be remarkably good. Both the vapor and the liquid branches of the numerical simulations are closely followed by the BH calculations, with an accuracy almost independent of the considered coverage, with the only exception of the Janus case ($\chi = 0.5$) that is however known to have an anomalous behavior [35], as remarked. This is only apparently in contrast with results from chemical potential, reported in previous Section VI A, where the BH results for chemical potential in the Janus case appeared to be less precise than in the SW case. On the one hand, a closer inspection reveals that BH results for each single coverage do indeed show a small quantitative discrepancy with the corresponding MC simulation, more or less uniform in the entire density-temperature plane. On the other hand, this latter feature constitutes an advantage in the method as a numerical solution of Eq.(4.4) may provide accurate coexistence lines if both the vapor and the liquid chemical potentials have similar inaccuracies. This results is, nonetheless, comparable in accuracy with those stemming from reference hypernetted chain (RHNC) integral equation theory [33, 34, 49], with the additional advantage of a less computational and algorithmical complexity and, more importantly, of being able to access the critical region, including the critical point, that is one of the main shortcomings common to all integral equation theories.

It is worth noticing how BH perturbation theory can provide an accurate prediction of the location of the coexistence lines even below the Janus limit, that is for $\chi < 0.5$, where extensive numerical simulations are so-far suggesting the fluid-fluid transition to be inhibited by a micellization process [36]. This could be useful for a future more focussed numerical calculation within a limited region of the phase diagram where BH theory predicts coexistence to occur.

C. The fluid-solid coexistence

Let us now turn to the fluid-solid coexistence, a calculation that has not been carried out so far for this model by any method. As illustrated in Sec.IV and below, BH perturbation scheme allows this analysis with an effort, both computational and algorithmical, comparable with that of the fluid-fluid case.

In the isotropic SW case with $\lambda = 1.5$, the reference point for this calculation are those obtained

as early as in 1980 by Young and Adler [50]. Using molecular dynamics (MD), they reported a detailed study of the different crystal structures (fcc, hcp, and bcc) with the corresponding Helmholtz free energies, thus arguing that fcc and hcp were the most stable structures within the entire temperature-density plane. Additional numerical simulations were later performed by Marr and Gast [51], Serrano-Illán and Navascués [52], and Kiselev *et al.* [53] essentially confirming this scenario. A very detailed study of the entire phase diagram of the SW, was carried out by Liu *et al.* [54].

In Fig.5, we report results from BH thermodynamic perturbation theory (solid line) along with results from Young and Adler (circles).

While at high temperatures all calculations agree, discrepancies start to appear on cooling away from the hard spheres limit. In particular, the plateau appearing in the solid branch of MD calculations indicates a fcc-fcc (or fcc-hcp) transition that is not accounted for in BH calculations, that assumed fcc structures all the way, although in principle it could be done. In the BH calculations, in particular, the difficulty arises from the stability of the numerical scheme used for the solution of Eqs.(4.6) and (4.7).

For lower coverages, no previous calculations on the Kern-Frenkel model exist to compare with. Fig.6 illustrate the coverage dependence of the fluid-solid coexistence lines as computed from MC simulations (points) and from BH thermodynamic perturbation theory (lines). As in the fluid-fluid case, MC simulations have been obtained up to the Janus fluid ($\chi = 0.5$), whereas BH theory provides results even below that limit. Simulations below the Janus limit could be done, but are computationally more demanding.

As in the SW case, even for lower coverages one might expect a structural transition at a certain density. Even assuming fcc to be the most stable structure, the range of the potential associated with the value $\lambda = 1.5$ used here, allows a fcc-fcc transition between one fcc with only nearest-neighbors bonded, and a more denser one with even the next-to-nearest-neighbors are bonded. This is associated with the jump in density that is present in some of the plots of Fig.6.

VII. CONCLUSIONS

In this paper we presented the first Barker-Henderson (BH) perturbative calculation for the one-patch Kern-Frenkel model, and compared with specialized MC simulations. The BH method hinges on a second-order thermodynamic perturbation theory in the inverse temperature, allowing the calculation of the Helmholtz free energy within this approximation, and hence, of all ther-

mododynamic quantities, such as the density and temperature dependence of pressure and chemical potential. A numerical solution has then been implemented to infer the fluid-fluid coexistence line (binodal) from the equality of pressure and chemical potential in the vapor and liquid phase at a given temperature. A similar procedure also provides the fluid-solid transition.

When compared with numerical simulations, the BH predictions are found to be extremely reliable in the entire phase diagram, and for all coverages from the isotropic SW potential to the lowest considered coverage ($\chi = 0.1$) very close to the hard-spheres limit. This constitutes one of the main advantages with respect to, in principle, superior and more accurate theoretical methodologies hinging on integral equation solutions, that are typically affected by the impossibility of accessing the critical region, and by the numerical instabilities occurring at low temperatures associated with low coverages. Even at the quantitative level, BH results were found to be competitive with integral equation theories, in agreement with previous results on the isotropic SW fluid.

The performance of BH is particularly noteworthy for coverages below the Janus limit, that is for $\chi < 0.5$, the most challenging region for numerical simulations in view of the tendency for the particles to form single and multi-layer clusters always exposing the hard-sphere surface in the outer region in order to maximize favorable contacts. This mechanism competes and destabilizes the condensation process and the interpretation of numerical simulation results become more and more obscure in that region. As a result, a clear scenario suggested by numerical simulations in this region is still missing. A better understanding could in principle be favored by our BH results that provide a well defined and restricted region of the temperature-density plane where indication of possible coexistences could be sought for.

While in the present paper the BH method has been applied to a single patch Kern-Frenkel potential, the method could potentially be extended to higher number of patches with no difficulties. As a matter of fact, this has already been done in Ref.[32] for two-patch colloids with Yukawa interactions for the attractive part. An inspection of the relevant equations (3.2) and (3.3), however, suggest the result to be identical to the one-patch case at the same coverage. This means that the BH method, in the present form, is not capable of distinguishing between one and two-patches, at the same coverage, a feature that, conversely, is accounted for in both numerical simulations [35, 36] and integral equation theory [33, 34]. In particular, it cannot then account for the anomalous behavior present in the Janus limit of the single patch [35] and not present in the corresponding coverage ($\chi = 0.5$) of the double patches model [36]. This is rather surprising in view of the fact that a similar method, based on a low-density virial expansion, applied to a companion problem, was able to distinguish between single and double patches, albeit with a rather poor estimate for the fluid-

fluid transition [55]. A promising approach in this respect appears to be the perturbative scheme devised for molecular fluids by Gubbins, Gray and others [2, 21], who considered an expansion in powers of the anisotropic part of the potential, in a way akin to that discussed in Appendix A, often supplemented by a Padé approximant to improve the convergence of the expansion, as proposed by Stell et al [58].

We plan to investigate this and other points in details in future work.

Acknowledgments

CG acknowledges the hospitality of Università Ca' Foscari of Venice where this work was started. FS and FR acknowledge support from ERC-226207-PATCHYCOLLOIDS.

Appendix A: The second order perturbation theory

As explained in Ref.[3], the most correct way of developing a perturbation expansion is in the grand-canonical ensemble. Assume a general potential of the form

$$\begin{aligned} U_\gamma(1, \dots, N) &= U_0(1, \dots, N) + \gamma U_I(1, \dots, N) \\ &= \sum_{i < j} \Phi_\gamma(ij) = \sum_{i < j} \Phi_0(ij) + \gamma \sum_{i < j} \Phi_I(ij), \end{aligned} \quad (\text{A1})$$

where $U_0(1, \dots, N) = \sum_{i,j} \Phi_0(ij)$ is the unperturbed part and $U_I(1, \dots, N) = \sum_{i,j} \Phi_I(ij)$ is the perturbation part. Here $0 \leq \gamma \leq 1$ is used as perturbativ parameter, and each coordinate i includes both the coordinate \mathbf{r}_i and patch orientation $\hat{\mathbf{n}}_i$, so that $i \equiv (\mathbf{r}_i, \hat{\mathbf{n}}_i)$. Also, $\beta = 1/(k_B T)$ denotes the inverse of the thermal energy.

Introducing the following short-hand notation

$$\int_{1, \dots, N} (\dots) \equiv \int \left[\prod_{i=1}^N d\mathbf{r}_i \langle (\dots) \rangle_{\omega_i} \right] \quad (\text{A2})$$

for the integration over all particle coordinates, the grand-canonical partition function

$$\mathcal{Q}_\gamma = \sum_{N=0}^{+\infty} \frac{e^{\beta\mu N}}{N! \Lambda_T^{3N}} \int_{1, \dots, N} e^{-\beta U_\gamma} = e^{-\beta \Omega_\gamma} \quad (\text{A3})$$

(here Λ_T is the de Broglie thermal wavelength, and Ω_γ is the grand-potential) can then be used to obtain an expansion of the Helmholtz free energy

$$F_\gamma = F_0 + \gamma \left(\frac{\partial F_\gamma}{\partial \gamma} \right)_{\gamma=0} + \frac{1}{2!} \gamma^2 \left(\frac{\partial^2 F_\gamma}{\partial \gamma^2} \right)_{\gamma=0} + \dots \quad (\text{A4})$$

as follows [3].

Taking the derivative of $\ln \mathcal{Q}_\gamma$ at fixed chemical potential μ , one has, using Eq.(A1)

$$\left[\frac{\partial}{\partial \gamma} \ln \mathcal{Q}_\gamma \right]_\mu = \frac{1}{2} \int_{1,2} \frac{\partial}{\partial \gamma} [-\beta \Phi_\gamma(12)] \rho_\gamma(12) , \quad (\text{A5})$$

where

$$\rho_\gamma(1 \dots h) = \frac{1}{\mathcal{Q}_\gamma} \sum_{N=h}^{+\infty} \frac{e^{\beta \mu N}}{(N-h)! \Lambda_T^{3N}} \int_{1, \dots, N} e^{-\beta U_\gamma} . \quad (\text{A6})$$

The second derivative is somewhat more laborious [3], and one obtains after some algebra

$$\begin{aligned} \left[\frac{\partial^2}{\partial \gamma^2} \ln \mathcal{Q}_\gamma \right]_\mu &= \frac{1}{2} \int_{1,2} \frac{\partial^2}{\partial \gamma^2} [-\beta \Phi_\gamma(12)] \rho_\gamma(12) + \frac{1}{2} \int_{1,2} \left(\frac{\partial}{\partial \gamma} [-\beta \Phi_\gamma(12)] \right)^2 \rho_\gamma(12) \\ &+ \int_{1,2,3} \frac{\partial}{\partial \gamma} [-\beta \Phi_\gamma(12)] \frac{\partial}{\partial \gamma} [-\beta \Phi_\gamma(23)] \rho_\gamma(123) \\ &+ \frac{1}{4} \int_{1,2,3,4} \frac{\partial}{\partial \gamma} [-\beta \Phi_\gamma(12)] \frac{\partial}{\partial \gamma} [-\beta \Phi_\gamma(34)] [\rho_\gamma(1234) - \rho_\gamma(12) \rho_\gamma(34)] . \end{aligned} \quad (\text{A7})$$

The free energy F_γ is then obtained by considering γ as an additional thermodynamical variable, and by performing the appropriate manipulations [3]. One then has

$$F_\gamma = \mu N - k_B T \ln \mathcal{Q}_\gamma , \quad (\text{A8})$$

and

$$N = k_B T \left[\frac{\partial}{\partial \mu} \ln \mathcal{Q}_\gamma \right]_\gamma , \quad (\text{A9})$$

where, for notational simplicity, here we do not distinguish between the canonical and grand-canonical number of particles N . Then

$$-k_B T \left[\frac{\partial}{\partial \gamma} \ln \mathcal{Q}_\gamma \right]_\rho = \left(\frac{\partial \Omega_\gamma}{\partial \gamma} \right)_\rho = \left(\frac{\partial \Omega_\gamma}{\partial \gamma} \right)_\mu - \left(\frac{\partial \Omega_\gamma}{\partial \mu} \right)_\gamma \left(\frac{\partial \rho}{\partial \gamma} \right)_\mu \left(\frac{\partial \mu}{\partial \rho} \right)_\gamma \quad (\text{A10})$$

and hence, using the chain rule

$$\left(\frac{\partial \rho}{\partial \gamma} \right)_\mu \left(\frac{\partial \gamma}{\partial \mu} \right)_\rho \left(\frac{\partial \mu}{\partial \rho} \right)_\gamma = -1, \quad (\text{A11})$$

one gets

$$-k_B T \left[\frac{\partial}{\partial \gamma} \ln \mathcal{Q}_\gamma \right]_\rho = -k_B T \left[\frac{\partial}{\partial \gamma} \ln \mathcal{Q}_\gamma \right]_\mu - k_B T \left[\frac{\partial}{\partial \mu} \ln \mathcal{Q}_\gamma \right]_\gamma \left(\frac{\partial \mu}{\partial \rho} \right)_\rho \quad (\text{A12})$$

that, with the help of Eq.(A9), leads to

$$\left(\frac{\partial F_\gamma}{\partial \gamma} \right)_\rho = -k_B T \left[\frac{\partial}{\partial \gamma} \ln \mathcal{Q}_\gamma \right]_\mu , \quad (\text{A13})$$

where the right-hand-side is given by Eq.(A5).

For the second derivative, one proceeds as before, to obtain

$$\left(\frac{\partial^2 F_\gamma}{\partial \gamma^2}\right)_\rho = -k_B T \left(\frac{\partial^2}{\partial \gamma^2} \ln \mathcal{Q}_\gamma\right)_\mu + k_B T \left[\left(\frac{\partial^2}{\partial \gamma \partial \mu} \ln \mathcal{Q}_\gamma\right)\right]_\gamma^2 / \left[\left(\frac{\partial^2}{\partial \mu^2} \ln \mathcal{Q}_\gamma\right)\right]_\gamma. \quad (\text{A14})$$

Using Eq.(A9) and the relation

$$\frac{\partial}{\partial \mu} = \rho \left(\frac{\partial \rho}{\partial P}\right) \frac{\partial}{\partial \rho}, \quad (\text{A15})$$

one finds

$$-k_B T \left[\frac{\partial^2}{\partial \gamma \partial \mu} \ln \mathcal{Q}_\gamma\right] = \rho \left(\frac{\partial \rho}{\partial P}\right) \frac{\partial}{\partial \rho} \left[\frac{1}{2} \frac{\partial}{\partial \gamma} [-\beta \Phi_\gamma(12)] \rho_\gamma(12)\right]. \quad (\text{A16})$$

Substituting in Eq.(A14), one finds

$$\left(\frac{\partial^2 F_\gamma}{\partial \gamma^2}\right)_\rho = -k_B T \left(\frac{\partial^2}{\partial \gamma^2} \ln \mathcal{Q}_\gamma\right)_\mu + \frac{N}{V^2} \left(\frac{\partial \rho}{\partial P}\right) \left\{ \frac{\partial}{\partial \rho} \left[\frac{1}{2} \frac{\partial}{\partial \gamma} [-\beta \Phi_\gamma(12)] \rho_\gamma(12)\right] \right\}^2, \quad (\text{A17})$$

where the first term on the right-hand-side is given by Eq.(A7).

The first and second order solutions, can be finally particularized to the potential form given in Eq.(A1), so that Eqs.(A5) and (A13) lead to

$$\left[\frac{\partial}{\partial \gamma} (\beta F_\gamma)\right]_{\gamma=0} = \frac{1}{2} \rho N \int d\mathbf{r}_{12} \langle \beta \Phi_I(12) \rangle_{\omega_1, \omega_2} g_0(12) \quad (\text{A18})$$

and Eqs.(A7) and (A17) leads to

$$\begin{aligned} \left(\frac{\partial^2}{\partial \gamma^2} (\beta F_\gamma)\right)_{\gamma=0} &= -\frac{1}{2} N \rho \int d\mathbf{r}_{12} \langle [-\beta \Phi_I(12)]^2 \rangle_{\omega_1, \omega_2} g_0(12) \\ &- N \rho^2 \int d\mathbf{r}_{12} d\mathbf{r}_{13} \langle [-\beta \Phi_I(12)] [-\beta \Phi_I(23)] \rangle_{\omega_1, \omega_2, \omega_3} g_0(123) \\ &- \frac{1}{4} N \rho^3 \int d\mathbf{r}_{12} d\mathbf{r}_{13} d\mathbf{r}_{14} \langle [-\beta \Phi_I(12)] [-\beta \Phi_I(34)] \rangle_{\omega_1, \omega_2, \omega_3, \omega_4} [g_0(1234) - g_0(12) g_0(34)] \\ &+ \beta N \left(\frac{\partial \rho}{\partial P}\right) \left\{ \frac{\partial}{\partial \rho} \left[\frac{1}{2} \rho^2 \int d\mathbf{r}_{12} \langle \Phi_I(12) \rangle_{\omega_1, \omega_2} g_0(12)\right] \right\}^2. \end{aligned} \quad (\text{A19})$$

Appendix B: The Barker-Henderson discrete representation

As in the spherically potential case, the above expressions are, however, not very useful for practical computation, due to the high complexity involved in the calculations of the three $g_0(123)$ and four $g_0(1234)$ point correlation functions.

Following the original work by Barker and Henderson, we return to the canonical partition function

$$Q = \frac{1}{N! \Lambda_T^{3N}} \int_{1, \dots, N} e^{-\beta U(1, \dots, N)} = \frac{1}{N! \Lambda_T^{3N}} Z = e^{-\beta F} \quad (\text{B1})$$

that is related to the configurational partition function Z and to the Helmholtz free energy F . The intermolecular distance axis r_{ij} is divided in intervals $(0, r_1), (r_1, r_2), \dots, (r_l, r_{l+1}), \dots$ in such a way that there are N_l distances in the l -th interval (r_l, r_{l+1}) . The total potential U appearing in Eq.(B1) can then be written as a sum over the different intervals with the respective multiplicity

$$U(1, \dots, N) = \sum_l N_l \bar{\Phi}(r_l, \{\Omega, \omega\}_l), \quad (\text{B2})$$

where $\bar{\Phi}(r_l, \{\Omega, \omega\}_l)$ is the average potential in the l -th interval (assumed to be constant), and $\{\Omega, \omega\}_l$ are the set of orientational angles included in the same interval.

Again we assume that the potential can be split into a hard-sphere part plus a tail

$$\bar{\Phi}(r_l, \{\Omega, \omega\}_l) = \bar{\phi}_0(r_l) + \bar{\Phi}_I(r_l, \{\Omega, \omega\}_l). \quad (\text{B3})$$

Introducing the average over the unperturbed system having Z_0 as configurational partition function

$$\langle \dots \rangle_0 = \frac{1}{Z_0} \sum_{N_1, N_2, \dots} \int_R d\mathbf{r}_1 \dots d\mathbf{r}_N e^{-\beta \sum_l N_l \bar{\phi}_0(r_l)}, \quad (\text{B4})$$

where the symbol R indicates that the integral is restricted to configurations having N_l intermolecular distances in the interval (r_l, r_{l+1}) , the Helmholtz free energy can be written in terms of that of hard-spheres F_0 as

$$\beta F = \beta F_0 - \ln \left\langle \left\langle e^{-\beta \sum_l N_l \bar{\Phi}_I(r_l, \{\Omega, \omega\}_l)} \right\rangle_{\{\omega\}} \right\rangle_0. \quad (\text{B5})$$

Note that the angular average over the $\{\Omega\}$ variables is included in the average (B4).

Use of the cumulant expansion

$$-\ln \langle e^{-\lambda x} \rangle = \lambda \langle x \rangle - \frac{1}{2} \lambda^2 \left(\langle x^2 \rangle - \langle x \rangle^2 \right) + \dots \quad (\text{B6})$$

leads to

$$\beta(F - F_0) = \beta F_1 + \beta F_2 + \dots, \quad (\text{B7})$$

where

$$\beta F_1 = \sum_l \left\langle \left\langle N_l \beta \bar{\Phi}_I(r_l, \{\Omega, \omega\}_l) \right\rangle_{\{\omega\}} \right\rangle_0, \quad (\text{B8})$$

and where

$$\beta F_2 = -\frac{1}{2} \sum_{lm} \left\langle \left\langle N_l N_m \beta \bar{\Phi}_I(r_l, \{\Omega, \omega\}_l) \beta \bar{\Phi}_I(r_m, \{\Omega, \omega\}_m) \right\rangle_{\{\omega\}} \right\rangle_0. \quad (\text{B9})$$

As [12],

$$\langle N_l \rangle_0 = 2\pi\rho N \int_{r_l}^{r_{l+1}} dr r^2 g_0(r), \quad (\text{B10})$$

the first order term becomes

$$\beta F_1 = \frac{1}{2}\rho N \int dr g_0(r) \langle \beta \Phi_I(r, \Omega, \omega_1, \omega_2) \rangle_{\omega_1, \omega_2} \quad (\text{B11})$$

that, of course, coincides with Eq.(A18).

For the second term (B9), an approximation is required as the effect of three and four-body interactions is included. Following Ref.[12], we assume molecules in different intervals to be uncorrelated

$$\langle N_l N_m \rangle_0 - \langle N_l \rangle_0 \langle N_m \rangle_0 = 0 \quad l \neq m, \quad (\text{B12})$$

and the fluctuations within a given interval, being related to the hard-spheres compressibility

$$\langle N_l^2 \rangle_0 - \langle N_l \rangle_0^2 = \langle N_l \rangle_0 k_B T \left(\frac{\partial \rho}{\partial P} \right)_0. \quad (\text{B13})$$

Substitution of Eqs.(B12) and (B13) into Eq.(B11), along with Eq.(B10), leads to

$$\beta F_2 = -\frac{1}{4}k_B T \rho N \left(\frac{\partial \rho}{\partial P} \right)_0 \int dr g_0(r) \langle [\beta \Phi_I(r, \Omega, \omega_1, \omega_2)]^2 \rangle_{\omega_1, \omega_2}, \quad (\text{B14})$$

which is the extension of the Barker-Henderson result [12] to angular dependent potentials.

Appendix C: Determination of the phase coexistence curves

To illustrate how the phase coexistence curves are found numerically, we consider in the following the phase separation into a gas and a liquid phase; the fluid-solid coexistence curve is determined correspondingly. Our aim is to solve Eqs. (4.3) and (4.4) for the two unknown particle densities ρ_g^* and ρ_l^* of the gaseous and liquidus phase, respectively. Using the common tangent construction, the concentration of the density of the gaseous and liquidus phase can be found geometrically [56]. In practice, however, ρ_g^* and ρ_l^* is determined numerically by solving Eqs. (4.3) and (4.4) simultaneously using a nonlinear root finding algorithm. To illustrate this procedure, we rewrite Eqs. (4.3) and (4.4) as

$$h_1(\rho_g^*, \rho_l^*) \equiv P_g^*(T^*, \rho_g^*) - P_l^*(T^*, \rho_l^*) = 0 \quad (\text{C1})$$

$$h_2(\rho_g^*, \rho_l^*) \equiv \mu_g^*(T^*, \rho_g^*) - \mu_l^*(T^*, \rho_l^*) = 0, \quad (\text{C2})$$

where we have introduced the functions $h_1(\rho_g^*, \rho_l^*)$ and $h_2(\rho_g^*, \rho_l^*)$. Since T^* is kept fixed in the following, we have written h_1 and h_2 as function of ρ_g^* and ρ_l^* only. By defining $\vec{x} = (\rho_g^*, \rho_l^*)^t$ and $\vec{h} = (h_1, h_2)^t$, where the subscript t denotes the transposed matrix, our task of finding the concentrations of the two coexisting phases at constant T^* is expressed in the form,

$$\vec{h}(\vec{x}) = 0. \quad (\text{C3})$$

This set of two nonlinear integral equation with two unknown variables is solved by using a well-tested implementation of the Newton-Raphson method [57], which solves Eq. (C3) iteratively as briefly described in the following. First, a start value \vec{x}_0 is chosen, and the gradient $\nabla\vec{h}(\vec{x}_0)$ is calculated. The new value \vec{x}_1 is found by a downhill step,

$$\vec{x}_1 = \vec{x}_0 - J^{-1}\vec{h}(\vec{x}_0). \quad (\text{C4})$$

Here, J is the Jacobian matrix which incorporates the partial derivatives of h_1 and h_2 . This step is repeated, $\vec{x}_1 \rightarrow \vec{x}_2 \rightarrow \vec{x}_3 \rightarrow \dots$, until the fix point $\vec{x}_n = \vec{x}^*$ with

$$\vec{h}(\vec{x}^*) = \vec{0}, \quad (\text{C5})$$

is found. It is important to note here that the root finding procedure requires the evaluation of $\vec{h}(\vec{x})$ at discrete points \vec{x}_i only. The nonlinear solver just steps down $\vec{h}(\vec{x})$ until Eq. (C3) is fulfilled to a prescribed threshold. Since the evaluation of $\vec{h}(\vec{x})$ at $\vec{x} = \vec{x}_i$ demands the calculation of several integrals, see Eqs.(3.2) and (3.3), $\vec{h}(\vec{x})$ cannot be expressed in an analytical form. Hence, the nonlinear solver calls a subroutine which calculates both the free energy and its gradient for each iteration step \vec{x}_i . The free energy is evaluated using the Chebyshev quadrature and the derivatives in Eq. (C4) are calculated using Ridder's implementation of Neville's algorithm [57].

After having found the two coexisting densities ρ_g^* and ρ_l^* at a given T^* , this procedure is repeated for a set of temperatures to map out the gas-liquid coexisting curve. The fluid-solid curve is calculated in exactly the same manner by equating the chemical potential and the pressure of the fluid and solid phase, Eqs. (4.6) and (4.7), respectively.

-
- [1] J. P. Hansen and I. R. McDonald, *Theory of Simple Liquids* (Academic, New York, 1986).
 - [2] C. G. Gray and K. E. Gubbins, *Theory of Molecular Fluids, Vol. 1: Fundamentals* (Clarendon, Oxford, 1984).
 - [3] D. Henderson and J.A. Parker, in *Physical Chemistry, an advanced treatise* Vol. VIIIA page 377 (1971)

- [4] J.A. Barker and D. Henderson, *Rev. Mod. Phys.* **48**, 587 (1976)
- [5] R. Zwanzig, *J. Chem. Phys.* **22**, 1420 (1954)
- [6] R. Zwanzig, *J. Chem. Phys.* **23**, 1915 (1955)
- [7] F. P. Buff and F. M. Schindler, *J. Chem. Phys.* **29**, 1075 (1958).
- [8] D. Chandler and J.D. Weeks, *Phys. Rev. Lett.* **25**, 149 (1970).
- [9] J.D. Weeks, D. Chandler, H.C. Andersen, *J. Chem. Phys.* **54**, 5237 (1971)
- [10] H. C. Andersen, D. Chandler and J.D. Weeks, *Adv. Chem. Phys.* **34**, 105 (1976)
- [11] D. Chandler, J.D. Weeks, and H.C. Andersen, *Science* **220**, 787 (1983)
- [12] J.A. Barker and D. Henderson, *J. Chem. Phys.* **47**, 2856 (1967)
- [13] D. Henderson, O. H. Scalise, and W. S. Smith, *J. Chem. Phys.* **72**, 2431 (1980)
- [14] N. Kern and D. Frenkel, *J. Chem. Phys.* **118**, 9882 (2003).
- [15] E. Bianchi, R. Blaak and C. N. Likos, *Phys. Chem. Chem. Phys.* **13**, 6397 (2011)
- [16] A. Lomakin, N. Asherie, and G. B. Benedek, *Proc. Natl. Acad. Sci. USA* **96**, 9465 (1999).
- [17] S. C. Glotzer, *Science* **306**, 419 (2004).
- [18] S. C. Glotzer and M. J. Solomon, *Nature Mater.* **6**, 557 (2007).
- [19] L. Verlet and J. J. Weis, *Mol. Phys.* **24**, 1013 (1972)
- [20] L. Verlet and J. J. Weis, *Mol. Phys.* **28**, 665 (1974)
- [21] K.E. Gubbins and C.G. Gray, *Mol. Phys.* **23**, 187 (1972); see also K.E. Gubbins and C. H. Twu, *Chem. Eng. Sci.* **33**, 863 (1981); C.G. Gray, K.E. Gubbins and C. H. Twu, *J. Chem. Phys.* **69**, 182 (1978)
- [22] J. Chang and S. I. Sandler, *Mol. Phys.* **81**, 745 (1994)
- [23] B. J. Zhang, S. Liang, and Y. Lu, *Fluid. Phase Equilibr.* **180**, 183 (2001)
- [24] R. Rotemberg, J. Dzubiella, J. P. Hansen and A. A. Louis, *Mol. Phys.* **102**, 1 (2004)
- [25] S. Zhou, *J. Chem. Phys.* **127**, 084512 (2007)
- [26] Y. V. Kalyuzhnyi, H. Docherty, and P. T. Cummings, *J. Chem. Phys.* **133**, 044502 (2010)
- [27] Y. V. Kalyuzhnyi, H. Docherty, and P. T. Cummings, *J. Chem. Phys.* **135**, 014501 (2011)
- [28] M. S. Wertheim, *J. Stat. Phys.* **35**, 34 (1984)
- [29] M. S. Wertheim, *J. Stat. Phys.* **42**, 495 (1986)
- [30] M. S. Wertheim, *J. Chem. Phys.* **85**, 2929 (1986)
- [31] M. S. Wertheim, *J. Chem. Phys.* **87**, 7323 (1987)
- [32] C. Gögelein, G. Nägele, R. Tuinier, T. Gibaud, A. Stradner, and P. Schurtenberger, *J. Chem. Phys.* **129**, 085102 (2008)
- [33] A. Giacometti, F. Lado, J. Largo, G. Pastore, and F. Sciortino, *J. Chem. Phys.* **131**, 174114 (2009).
- [34] A. Giacometti, F. Lado, J. Largo, G. Pastore, and F. Sciortino, *J. Chem. Phys.* **132**, 174110 (2010)
- [35] F. Sciortino, A. Giacometti, and G. Pastore, *Phys. Rev. Lett.* **103**, 237801 (2009).
- [36] F. Sciortino, A. Giacometti, and G. Pastore, *Phys. Chem. Chem. Phys.* **12**, 11869 (2010).
- [37] N. Carnahan and K. E. Starling, *J. Chem. Phys.* **51**, 635 (1969)
- [38] G. Nägele, *The Physics of Colloidal Soft Matter*, Lecture Notes Vol. 14 (Institute of Fundamental

Technological Research/Polish Academy of Science, Warsaw, Poland 2004)

- [39] M. S. Wertheim, Phys. Rev. Lett. **10**, 321 (1963)
- [40] G. J. Throop and R. J. Bearman, J. Chem. Phys. **42**, 2408 (1965)
- [41] W.W. Wood, J. Chem. Phys. **20**, 1234 (1952)
- [42] J. M. Kincaid and J. J. Weis, Mol. Phys. **34**, 931 (1977)
- [43] D. A. Kofke, J. Chem. Phys. **98**, 4149 (1993)
- [44] C. Vega and E. Sanz and J. L. F. Abascal and E. G. Noya, J. Phys.: Condens. Matter, **20**, 153101 (2008).
- [45] F. Romano and E. Sanz and F. Sciortino, J. Chem. Phys., **132**, 184501 (2010).
- [46] F. Lado, Mol. Phys. **47**, 283 (1982).
- [47] F. Lado, Mol. Phys. **47**, 299 (1982).
- [48] F. Lado, Phys. Lett. **89A**, 196 (1982).
- [49] A. Giacometti, G. Pastore, and F. Lado, Mol. Phys. **107**, 555 (2009).
- [50] D. A. Young and B. J. Adler, J. Chem. Phys. **73**, 2430 (1980)
- [51] D. W. Marr, and A. P. Gast, J. Chem. Phys. **99**, 2024 (1993)
- [52] J. Serrano-Illán, and G. Navascués, Phys. Rev. E **73**, 011110 (2006)
- [53] S. B. Kiselev, J. F. Ely, and J. R. Elliott JR, Mol. Phys. **104**, 2545 (2006)
- [54] H. Liu, S. Garde, S. Kumar, J. Chem. Phys. **123**, 174505 (2005)
- [55] R. Fantoni, D. Gazzillo, A. Giacometti, M. A. Miller, and G. Pastore, J. Chem. Phys. **127**, 234507 (2007).
- [56] M. Dijkstra, R. van Roij, and R. Evans, Phys. Rev. E **59**, 5744 (1999)
- [57] W. H. Press, S. A. Teukolsky, W. T. Vetterling, and B. P. Flannery, *Numerical Recipes in C*, 2nd ed., (Cambridge University Press, New York, 1992)
- [58] G. Stell, J.C. Rasaiah, and H. Nagaran, Mol. Phys. **27**, 1393 (1974)

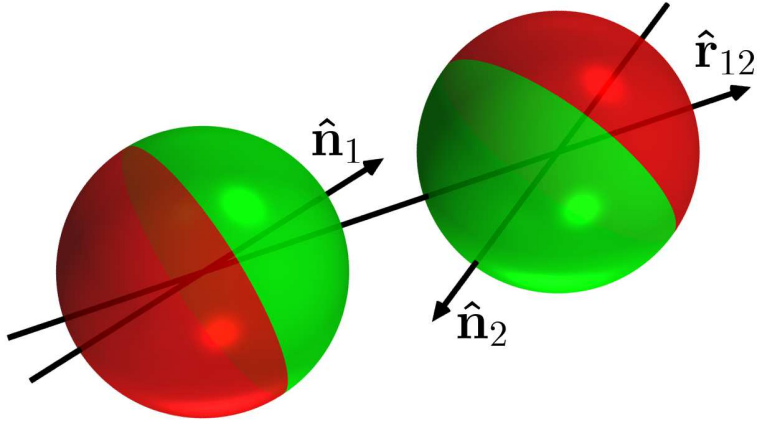


FIG. 1: The Kern-Frenkel potential in the case of a single patch. The surface of each sphere is partitioned into an attractive part (color code: green) and a repulsive part (color code: red). Units vectors $\hat{\mathbf{n}}_1$ and $\hat{\mathbf{n}}_2$ identify the directions of each patch, whereas the unit vector $\hat{\mathbf{r}}_{12}$ join the centers of the two spheres, directed from sphere 1 to sphere 2. The particular case shown corresponds to a 50% fraction of attractive surface (coverage $\chi = 0.5$).

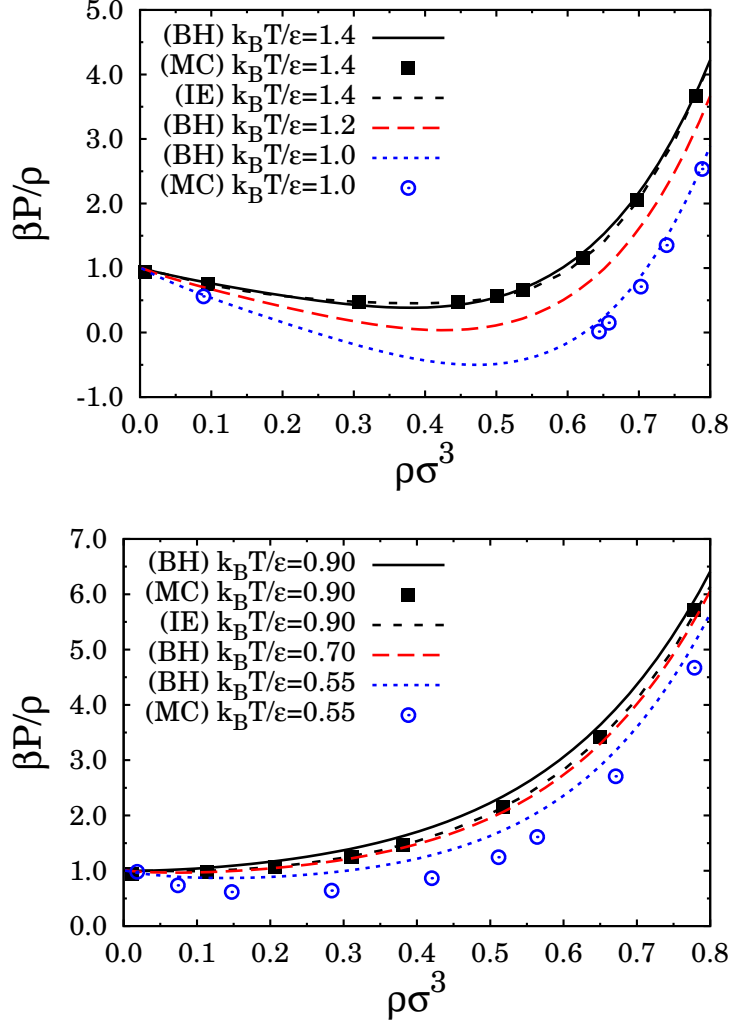


FIG. 2: Reduced pressure $\beta P/\rho$ as a function of reduced density $\rho\sigma^3$ in the case of a square-well fluid with coverage $\chi = 1$ (top panel), and in the case of a Janus fluid with coverage $\chi = 0.5$ (bottom panel). A value of $\lambda = 1.5$ is used. Results from BH thermodynamic perturbation theory (BH) are compared with Monte Carlo simulation (MC) and with RHNC integral equation theory (IE). Different curves refer to different temperatures as shown.

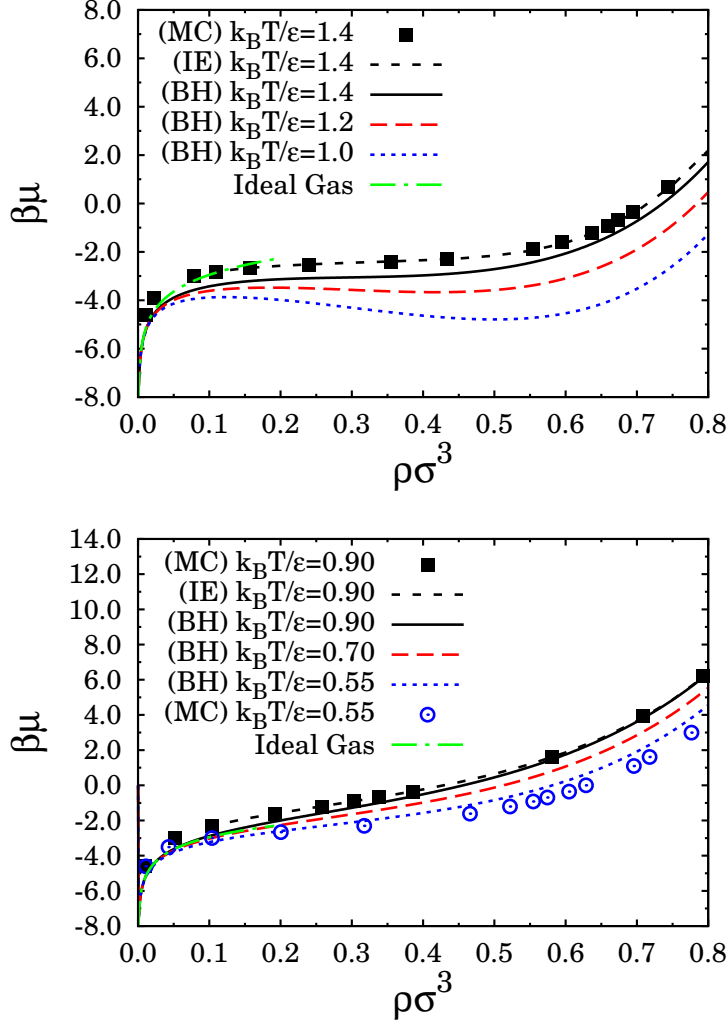


FIG. 3: Reduced chemical potential $\beta\mu$ as a function of reduced density $\rho\sigma^3$ in the case of a square-well fluid with coverage $\chi = 1$ (top panel), and in the case of a Janus fluid with coverage $\chi = 0.5$ (bottom panel). A value of $\lambda = 1.5$ is used. Results from BH thermodynamic perturbation theory (BH) are compared with Monte Carlo simulation (MC) and with RHNC integral equation theory (IE). Different curves refer to different temperatures as indicated. The low-density ideal gas limit (light dashed line) is also depicted.

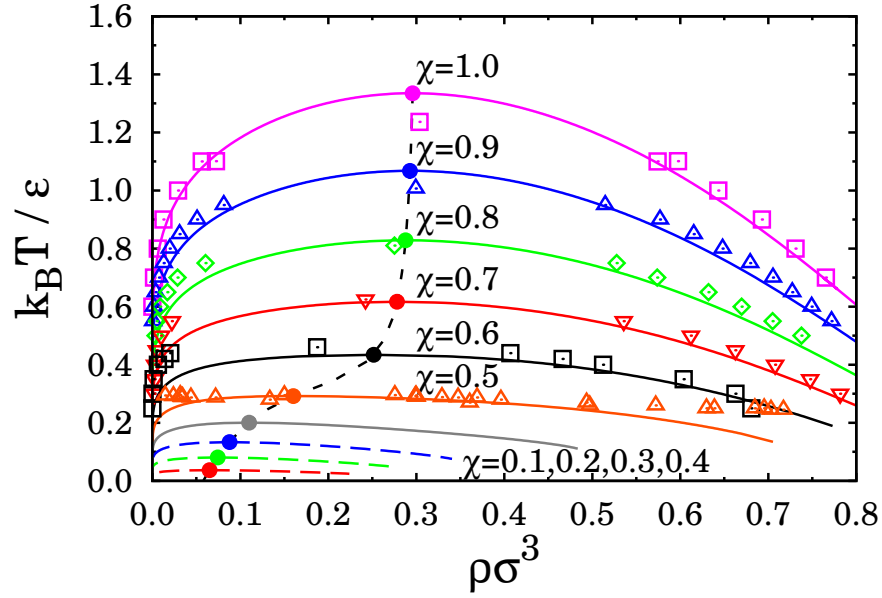


FIG. 4: The fluid-fluid coexistence curves as computed from BH perturbation theory and compared against numerical simulations. Lines are from perturbation theory, points from numerical simulations, for $\lambda = 1.5$ from Ref. [36]. All coverages from $\chi = 1.0$ (SW case) to $\chi = 0.0$ (HS case) are depicted in the former case, whereas numerical simulations are in the range $0.5 \leq \chi \leq 1.0$, that is from the Janus to the SW limit.

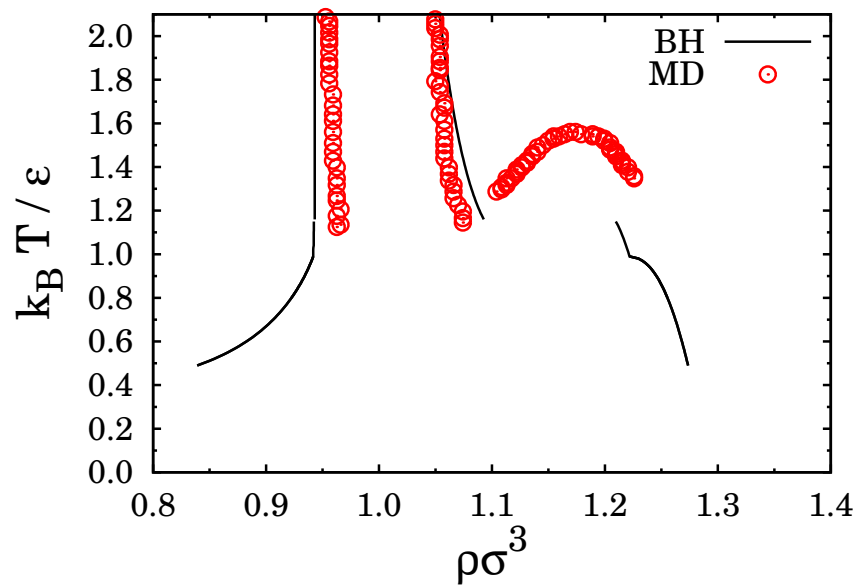


FIG. 5: Fluid-solid coexistence for the case of the SW potential ($\chi = 1.0$) with $\lambda = 1.5$. Results from Barker-Henderson (BH) perturbation theory are contrasted with molecular dynamics (MD) data by Young and Adler [50].

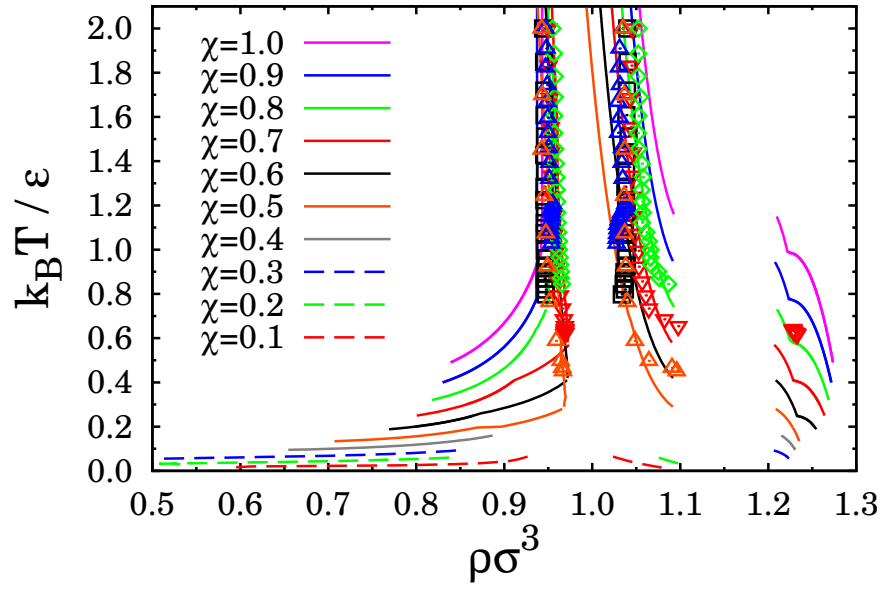


FIG. 6: Coverage dependence of the fluid-solid coexistence curves. Again $\lambda = 1.5$ and considered coverages are from $\chi = 1.0$ (SW case) to $\chi = 0.1$ for Barker-Henderson perturbation theory (lines) and from $\chi = 0.9$ to $\chi = 0.5$ (Janus) for Monte Carlo simulations.